NON-CONTACT GAS TURBINE BLADE VIBRATION MEASUREMENT FROM CASING PRESSURE AND VIBRATION SIGNALS – A REVIEW

Gareth L. Forbes
School of Mechanical and Manufacturing Engineering, The University of New South Wales
Sydney, NSW, Australia

Robert B. Randall
School of Mechanical and Manufacturing Engineering, The University of New South Wales
Sydney, NSW, Australia

ABSTRACT

This paper presents a summary of a recent research program, focusing on a new method of non-contact gas turbine blade vibration measurement using casing pressure and vibration signals. Currently the dominant method of non-contact measurement of turbine blade vibrations employs the use of a number of proximity probes located around the engine periphery measuring the blade tip (arrival) time (BTT). Despite the increasing ability of this method there still exist some limitations, viz: the requirement of a large number of sensors for each engine stage, difficulties in dealing with multiple excitation frequencies, sensors being located in the gas path, and the inability to directly measure the natural frequency of a given blade.

Simulations established with a physics based model along with experimental measurements are presented in this paper, using internal pressure and casing vibration measurements, which have the potential to rectify some of these problems.

INTRODUCTION

The greatest cause of failures in gas turbines comes from blade faults, reported to be up to 42% of total gas turbine failures [1]. Blade vibration is unavoidable and inherent in the operation of any gas turbine and without proper design for the excitation forces present, blade vibrations can be a cause of blade degradation and lead to failure. It is paramount that blade vibration can be measured and blade fatigue be estimated in the design stage. High cycle fatigue (HCF) from these inherent blade vibrations is the largest single cause of component failures in modern military aircraft gas turbine engines, exceeding the number attributed to low cycle fatigue, corrosion, overstress, manufacturing processes, mechanical damage, and materials [2]. Another prominent need that has arisen, which requires the specific measurement of blade vibration in current turbines, is the situation when they are run beyond their design life or are subject to different conditions from those for which they were originally designed. For instance, some electricity plants in the Asia Pacific region are facing the dilemma of having to run their turbines beyond the original manufacturer's recommended running hours in order to continue to provide an uninterrupted electricity supply [3]. It is clear that gas turbine blade vibration measurement is essential.

Gas turbine blade vibration measurement is thus motivated by the desire to acquire two principal pieces of information, either the blade's forced vibration magnitude and frequency, or to estimate the modal parameters of the blade. The impetus for this information is generally driven, respectively, by the need for knowledge of HCF estimates for blade life, or the use of blade modal parameter values for condition monitoring of the blades.

Measurement of blade vibration can be achieved with the direct attachment of strain gauges to the blade surface, however the attachment of sensors to all blades within the engine is never desirable, and is certainly not practical outside of the design stage. This is due not only to the cost of instrumenting each blade, but additionally because of the complexities of bringing the measured signals to an external monitoring device. This needs to be done either with the use of slip rings or a wireless telemetry system. Strain gauges are also located on the engine working surface areas, such that they affect the aerofoil surface, and are exposed to the harsh internal engine environment, this not being conducive to sensor longevity.

Such are the difficulties of direct measurement of blade vibration, non-contact blade vibration measurement has been sought, with BTT methods showing the most promise and receiving research attention since the 1970's. Despite the promise of BTT methods they are still not without limitations or shortcomings four decades after their initial use.

It was recently proposed that blade vibration would have an affect on the casing wall pressure and casing vibration, and thus measurement of these parameters could be used for monitoring of blade vibration parameters [4]. The ensuing research program which was undertaken to follow up this proposal is reviewed in this paper. The presented work may be divided into three sections, these being:

(i) Direct measurement of blade vibration amplitudes, which could be used for estimating blade HCF as first proposed in Ref. [5], by phase demodulating the measured internal casing pressure. Results are shown herein for simulated turbine pressure signals.

(ii) The proposition of indirectly measuring rotor blade natural frequencies by varying the rotation speed such that the blade excitation traversed the blade natural frequency, allowing an observable increase in the casing vibration spectrum at this engine speed, was given in Ref. [4]. The results from simulated casing vibration signals using this indirect blade natural frequency measurement are given.

(iii) Lastly, it was suggested that rotor blade natural frequencies could be measured directly from the stochastic casing vibration response [6], and this was later verified experimentally [7]. Both analytical and experimental results obtained from the above research are presented.

ROTOR BLADE PRESSURE PROFILE AND MOTION

Firstly, the generation of the internal pressure inside a gas turbine and the associated rotor blade motion will be derived, since all the following analysis techniques are based on this derivation.

As stated earlier, blade vibration in a gas turbine is inherent and unavoidable. This inevitable blade vibration develops from the unsteady pressure field through which the rotor blades pass during rotation. It is initiated by the transfer of the internal gas passing from rotating to stationary frames of reference as it passes through different engine stages. This can be visualised with the aid of a 1.5 stage turbine schematic as in Fig. 1. It is evident as the fluid passes from the inlet to the outlet though the inlet guide vanes (IGV's), through the rotor stage, and finally through the stator stage the change in fluid rotation will cause fluctuating forces on all the blades inside the engine, and thus will cause them to vibrate. Generally rotor blades will be excited by dominant frequencies at stator passing frequencies (SPF).

The excitation on the r^{th} blade could then be mathematically described as:

$$f(t)_r = F_0\left\{\sum_{q=0}^{\infty} C_q \cos\left[q\left(\Omega t + \gamma_q + \gamma_r\right)\right]\right\} \qquad (1)$$

The above force can be of any shape depending on the selected Fourier series co-efficients of C_q, γ_q.

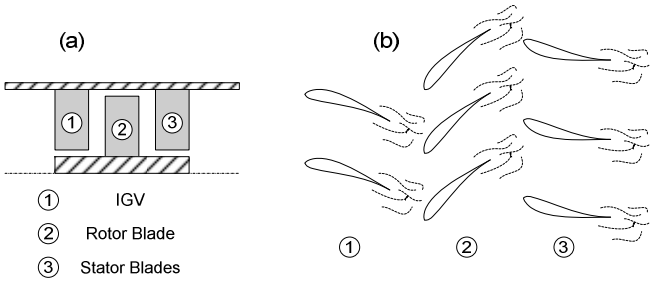

Fig. 1 (a) longitudinal section of 1.5 stage turbine, (b) cross section of 1.5 stage turbine showing wake interaction between blade rows

Along with the fluctuating pressure forces on the blades causing them to vibrate, the rotor blades and indeed the stator blades will have a static pressure profile which will develop as the fluid passes over the blade aerofoil surface. With this knowledge of the pressure interaction inside a gas turbine, analysis of the casing pressure and vibration signals will now be shown in order to achieve the reconstruction of some of the blade vibration parameters.

PHASE DEMODULATION OF INTERNAL PRESSURE SIGNAL

If a blade is excited by one single dominant discrete frequency, then the motion of the blade tip for the r^{th} blade can be stated, without loss of generality, as:

$$x(t)_r = X_k \sin(k\Omega(t) + \gamma_k) \qquad (2)$$

For the case of synchronous vibration in a gas turbine, k is a positive integer and is often referred to as the engine order of excitation. If the blades have well separated modes and the excitation lies relatively close to one of the natural frequencies then X_k and γ_k can found from the solution of the forced vibration of the single degree of freedom system for the mode of interest of the rotor blade.

With the assumption that the time averaged pressure profile around any blade is constant, the pressure profile around any blade can be described by a harmonic series, given by:

$$P_r = \mathrm{Re}\left\{\sum_{i=0}^{\infty} A_i P e^{ji[\theta+\Omega(t)+\alpha_r+\gamma_i]}\right\} \qquad (3)$$

where $j = \sqrt{-1}$ and A_i and γ_i are the amplitude and phase of the corresponding Fourier series. It is seen that equation (3) is a rotating wave form of any shape depending on the selected Fourier series co-efficients of A_i, γ_i and initial phase offset of α_r. For instance in Fig. 2 a pressure profile shape is plotted, consisting of a raised cosine which spans one half blade spacing before and after each blade, for 6 rotor blades.

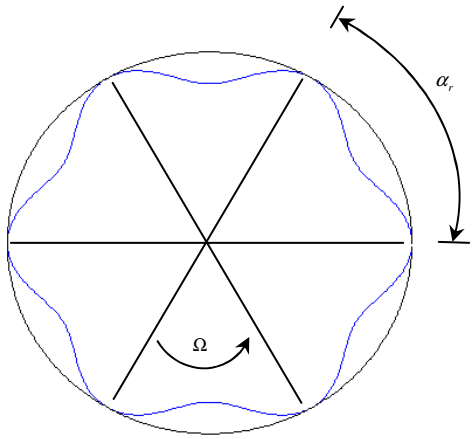

Fig. 2 Schematic of simple first harmonic pressure distribution for a 6 bladed arrangement without blade motion

If we now make the assumption that the pressure profile around one blade follows the motion of that blade when it vibrates around its equilibrium position, then the pressure

profile for the r^{th} blade will be modulated by the blade motion $x(t)_r$ such that the pressure profile can now be written as:

$$P_r = \mathrm{Re}\left\{\sum_{i=0}^{\infty} A_i P e^{ji[\theta+\Omega(t)+x(t)_r+\alpha_r+\gamma_i]}\right\} \quad (4)$$

If we implement the Laurent power series expansion of an exponential function in terms of Bessel functions:

$$e^{x/2(t-1/t)} = \sum_{n=-\infty}^{\infty} J_n(x)t^n \quad (5)$$

then it can be seen that P_r is in the form of equation (5), such that P_r can now be written as:

$$P_r = \mathrm{Re}\left\{\sum_{i=0}^{\infty} A_i P e^{ji[\theta+\Omega(t)+\alpha_r+\gamma_i]} \sum_{n=-\infty}^{\infty} J_n\left(iX_k\right) e^{jn[k\Omega(t)+\gamma_k]}\right\} \quad (6)$$

Now taking the real part for all harmonics

$$P_r = \sum_{i=0}^{\infty}\sum_{n=-\infty}^{\infty} A_i P J_n(iX_k)\cos\begin{bmatrix} i(\theta+\Omega(t)+\alpha_r+\gamma_i) \\ +n(k\Omega(t)+\gamma_k)\end{bmatrix} \quad (7)$$

As the measured pressure at the casing wall, mathematically represented in equation (7), is a phase modulated signal, then phase demodulation would result in obtaining information about the modulating frequency i.e. $x(t)_r$ and the tip deflection X_k. It is on this simple premise of the phase demodulation of the internal pressure that it is proposed that information about rotor blade vibration can be obtained. However the phase demodulation of the signal, as given in equation (7), is not a straightforward process as this type of signal violates some assumptions for use with conventional demodulation techniques. For conventional phase demodulation, the maximum modulation frequency must certainly be less than half the carrier frequency to avoid aliasing. It can be seen that for the internal pressure signal this assumption will never be satisfied, as multiple carrier frequencies exist at harmonics of shaft speed, with the modulating frequency itself also a multiple of shaft speed. How to overcome the aliasing and demodulation problems of a signal of this type will now be introduced.

A simplified example

If we look at the special case of $k = s$, where s is the number of stator blades, and $\gamma_k = 0$, then:

$$k\Omega = s\Omega = \omega_{spf}$$

For illustration, if we also limit $i < s$ then we can see the spectrum of the pressure signal will be a sum of discrete harmonics of i with sets of sidebands at $\pm\ \omega_{spf}$. For instance the frequency at Ω will be made up of a component from Ω and $-(s-1)\Omega+\omega_{spf}$, see Fig. 3

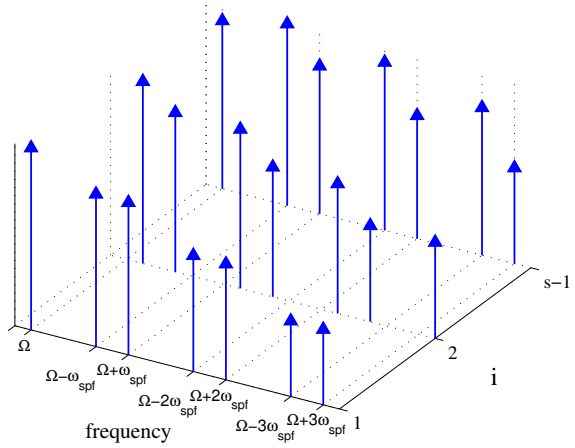

Fig. 3 Discrete spectrum for carrier frequencies *i* and modulating sidebands $\pm\ \omega_{spf}$.

Values of the measured pressure signal spectrum can be taken at frequency locations of $\Omega, \omega_{spf}-\Omega, \omega_{spf}+\Omega$, these being respectively y_1, y_{s-1}, y_{s+1}.

$$\begin{aligned} y_1 &= A_1 P J_0\left(X_s\right) + A_{(s-1)} P J_{-1}\left[(s-1)X_s\right] \\ y_{s-1} &= A_1 P J_{-1}\left(X_s\right) + A_{(s-1)} P J_0\left[(s-1)X_s\right] \\ y_{s+1} &= A_1 P J_1\left(X_s\right) + A_{(s-1)} P J_{-2}\left[(s-1)X_s\right] \end{aligned} \quad (8)\text{-}(9)$$

$A_1 P, A_{(s-1)} P, X_s$ are all unknowns. Now writing equations (8)-(9) in matrix form:

$$\mathbf{y} = \mathbf{D}\mathbf{x} \quad (11)$$

$$\mathbf{y} = \begin{bmatrix} y_1 & y_{s-1} & y_{s+1}\end{bmatrix}^T \qquad \mathbf{x} = \begin{bmatrix} A_1 P \\ A_{(s-1)} P\end{bmatrix} \quad (12)\text{-}(13)$$

$$\mathbf{D} = \begin{bmatrix} J_0\left(X_s\right) & J_{-1}\left[(s-1)X_s\right] \\ J_{-1}\left(X_s\right) & J_0\left[(s-1)X_s\right] \\ J_1\left(X_s\right) & J_{-2}\left[(s-1)X_s\right]\end{bmatrix} \quad (14)$$

Although (11) is not linear, it is linear for any value of X_s and can be solved by the linear least squares optimization of the over-determined system of equations (12)-(14). The estimate for the unknown co-efficients at any value of X_s is given, in the least squares sense, by: [8]

$$\hat{\mathbf{x}} = \left(\mathbf{D}^{\mathrm{T}}\mathbf{D}\right)^{-1}\mathbf{D}^{\mathrm{T}}\mathbf{y} \quad (15)$$

To find the optimal value of X_s to fit the system of equations, the non-linear least squares grid search is undertaken to maximise $g\left(x\right)$ [8], where

$$g(x) = \mathbf{y}^{\mathrm{T}}\mathbf{D}\left(\mathbf{D}^{\mathrm{T}}\mathbf{D}\right)^{-1}\mathbf{D}^{\mathrm{T}}\mathbf{y} \qquad (16)$$

A signal, of the type expressed in equation (7), that does not conform to the general requirements of conventional phase demodulation can therefore be demodulated with a non-linear least squares grid search fit of the spectrum.

The system is further complicated when noise is present in the signal; however utilising two measurement locations at a known angular offset from each other, this limitation can be overcome. Further results and complete derivation of the non-linear least squares grid search phase demodulation algorithm can be found in Refs. [5, 9].

Implementation with more realistic pressure signal

Now creating a more realistic internal turbine pressure signal with values as given in Table 1, substituted into equation (4), with a single known dominant rotor blade driving frequency at SPF, the results for the estimation of the rotor blade vibration amplitude are shown in Fig. 4

It can be seen that for the simulated signal with realistic amounts of noise the amplitude is generally estimated to within a 10% error for SNR ratios less than 3. The normalised grid spacing refers to a decreasing spacing between estimated values of X_k for which the least squared error is minimal over the variable space.

Table 1. Parameter values for the example with more realistic input values.

X_k (rad)	No. of stator blades	No. of rotor blades	max 'i' carrier harmonics	α_r (rad)	γ_k (rad)	Ω (Hz)
0.01	6	19	48	$\frac{\pi}{19}$	$\frac{\pi}{7}$	10

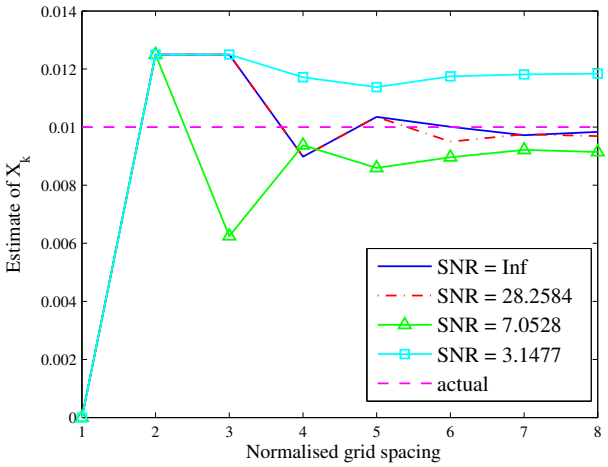

Fig. 4 Convergence of X_k estimate for increasing normalised grid spacing with parameters from Table 1 with increasing SNR as shown. Actual value of X_k also as shown.

It should be noted that phase demodulation of the internal pressure signal to estimate actual rotor blade vibration amplitudes requires the assumption to be met that the pressure at the blade tip is reasonably un-altered compared with that at the casing surface.

INDIRECT MEASUREMENT OF BLADE NATURAL FREQUENCIES FROM CASING VIBRATIONS

As non-intrusive measurement of blade condition within a gas turbine is the goal of most condition monitoring of these systems, a method of measuring blade vibration parameters without the need to place any sensors in the gas flow path would be optimal. It will now be shown that the blade natural frequencies of the rotor blades may be estimated indirectly by sweeping the engine speed over a range of speeds, such that engine order excitation frequencies excite the blade natural frequency. This method is similar to the indirect BTT methods [10, 11] which use the same engine sweeping technique, to monitor a blade's natural frequency so that it could subsequently be used to monitor blade structural degradation.

Only one other author is known to have previously attempted to find a correlation between casing vibration and blade condition [12]. Mathioudakis et al [12] used an inverse filtering technique to reconstruct the internal pressure signal within a gas turbine from the measured casing vibrations by constructing transfer functions between the two signals. This demonstrated that the internal pressure signal and casing vibrations are indeed correlated to one another.

The proposed method of measuring casing vibrations to determine blade vibration characteristics has a discernible advantage over current tip timing techniques, as it does not require perforation of the casing, lending itself to much easier application to existing, and in the design of new, turbines.

The casing of a gas turbine, under test conditions, can be excited by two groups of forces [12], viz: (a) forces from the engine and running gear through casing/bearing attachments, (b) forces from the aerodynamic/structural interaction within the engine. The second group of forces, (b), understood to be dominant, can then be further broken down into its presumed constituents; (i) interaction with the rotating pressure profile around each rotor/stator blade, (ii) propagation of acoustic waves inside the casing, (iii) pressure fluctuations due to turbulent and impulsive flows.

If the first constituent of the second group of forces, viz (b)(ii), is highlighted then it can be seen that this excitation force arises from the rotating internal pressure which was derived in the previous section and is given in its most general form in equation (4). These forces are the dominant contributor to the deterministic casing wall pressure and vibration.

Essentially the casing vibration will act in a similar manner to the internal casing pressure which drives its motion, after it has passed through the linear time invariant (LTIV) filter of the casing structural transfer function. The mathematical derivation of the casing vibration will not be given here for brevity but can be found in Refs. [6, 9]. The properties present in the casing vibration spectrum can however be discussed with respect to the casing pressure, as the transfer through the casing will only provide an amplitude and phase modification of the pressure signal.

Deterministic casing vibration for a simulated turbine

Casing vibration results are shown for a simulated turbine with the parameters given in Table 2. The blades are modelled as uncoupled single degree of freedom spring/mass/damper systems, with a dominant excitation frequency at SPF assumed to be only exciting a single blade mode with a nominal natural frequency of 500Hz. Shown in Fig. 6 is the deterministic casing vibration response for a simulated turbine when the casing is modelled as a circular ring under the influence of an internal pressure signal, of the same form as that given in equation (4), for an engine speed of 80Hz. Inspection of equation (4) and Fig. 6 shows that discrete harmonics of engine speed will be present. As the engine speed is swept over a range such that the excitation frequency, $5\,\Omega$, traverses the blade natural frequency, 500Hz, the displacement of the rotor blade vibration will be increase as will the harmonics of the engine speed, especially the excitation frequency sidebands, these being $\mathrm{BPF}\pm\mathrm{SPF}$. Thus, if a waterfall plot is made of the deterministic casing response spectrum over a range of running speeds, an increase in the engine speed harmonics will be seen when the blade natural frequency is excited, in this case when $\Omega = 100\mathrm{Hz}$, as can be seen in Fig. 5. This increase is most evident when observing the first positive SPF sideband, which is indicated, and with the first SPF sideband plotted in Fig. 7 over the range of engine speeds. The increase in sideband amplitude is very evident in Fig. 7 by the increase in amplitude when the natural frequency is traversed.

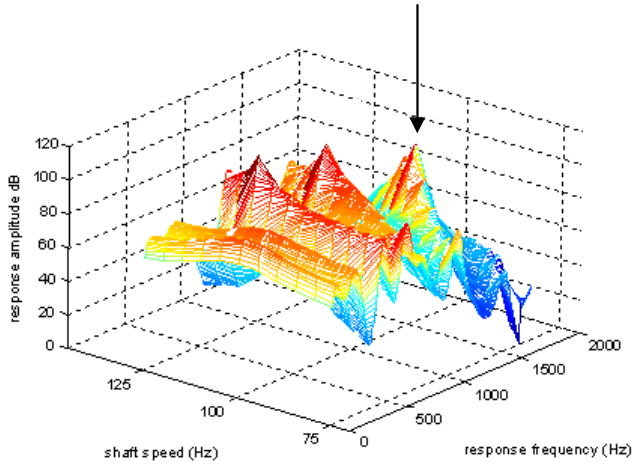

Fig. 5 Waterfall plot of analytical casing response spectrum for engine shaft speed of 75-125 Hz. The analytical model consists of 6 rotor blades 5 stator blades with a rotor blade natural frequency of 500Hz. Indicated by the arrow is the increase in the first positive SPF sideband when the blade natural frequency is traversed.

Table 2. Parameter for simulated turbine

Rotor blade natural frequency (Hz)	Swept engine speeds (Hz)	No. of stator blades	No. of rotor blades
500	75-125	5	6

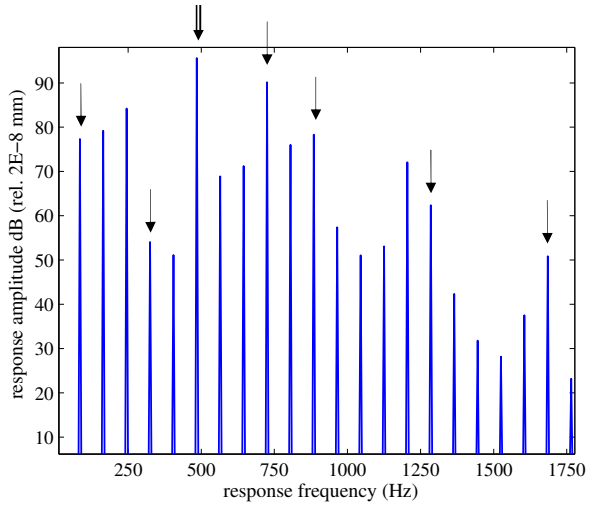

Fig. 6 Analytic casing radial response at 80Hz shaft speed in reference to Fig. 5. Indicated by double arrow is BPF, other arrows indicate $\mathrm{BPF}\pm\mathrm{SPF}$

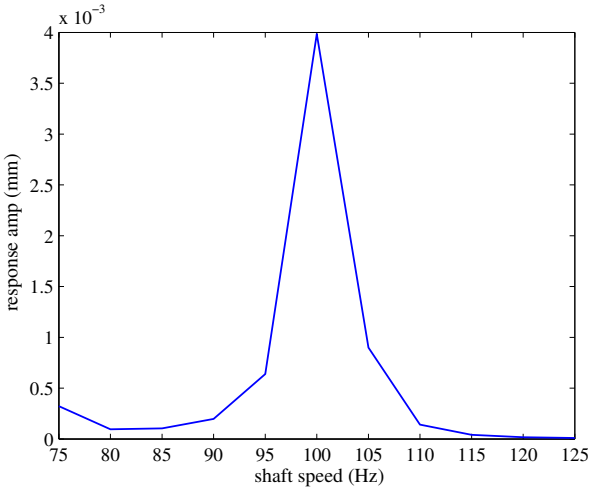

Fig. 7 First positive SPF sideband amplitude plotted against the shaft input speed. Clearly indicated is the peak in the response amplitude when the blade natural frequency is traversed by the force frequency being 5Ω.

DIRECT MEASUREMENT OF BLADE NATURAL FREQUENCIES FROM CASING VIBRATIONS

It was shown that the indirect measurement of rotor blade natural frequencies could be achieved by observing the deterministic portion of the turbine casing vibration signal as the engine speed is swept over a range of speeds. It would however be much less restrictive if the blade natural frequency estimates could be achieved from casing vibration measurements at any given engine running speed. This has been shown to be achievable if the stochastic portion of the turbine casing response is observed instead.

As inherent as blade vibration is in the running of a gas turbine engine, so is the presence of turbulence in the fluid flow within the engine. This turbulence will also drive blade motion along with the deterministic pressure forces. The force on any rotor blade can then be described, including stochastic forces and driven predominantly by stator pass harmonics as:

$$f(t)_r = F_0[b(t)]\left\{\sum_{q=0}^{\infty} C_q \cos\left[q\left(\omega_{spf}t + \gamma_q + \gamma_r\right)\right]\right\} \qquad (17)$$

the Fourier co-efficients can be given values to describe any shaped impulse. $b(t)$ is modelled as a white random variable with zero mean, however in practice the turbulence will be somewhat bandlimited and coloured.

As before if the rotor blades are modelled as a single degree of freedom system, the spectrum of the blade motion will result from the multiplication of the force spectrum, which will display the same first order statistics as that of the random variable $b(t)$, and the blade transfer function. The spectrum of the blade motion will thus be stochastic in nature and in the ensemble average response the blade motion spectrum will correspond with that of the amplitude of the blade transfer function. This process is shown schematically in Fig. 8 with the instantaneous spectrum of the blade force, equation (17), multiplied by the blade transfer function resulting in the instantaneous spectrum of the blade response.

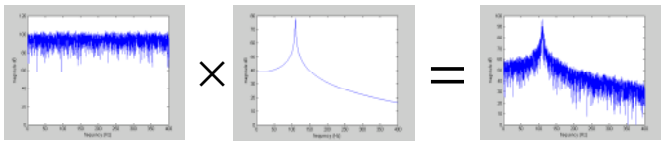

Fig. 8 Schematic of the derivation the stochastic blade forced motion

Now that the blade motion is known, the internal pressure under the influence of the stochastic blade motion can be derived, observing equation (4) it can be seen that this equation can be rearranged as:

$$P_r = \mathrm{Re}\left\{\sum_{i=0}^{\infty} A_i P e^{j\left[\theta+\Omega t+\alpha_r+\gamma_i\right]} e^{j\left[x(t)_r\right]}\right\} \qquad (18)$$

The left-hand component of the exponential function in equation (18) is deterministic and its spectrum will be a discrete set of harmonics of shaft speed, Ω. The spectrum of the real part of the right-hand component of the exponential function in equation (18), will have the same form as the spectrum of the blade motion $x(t)_r$. The spectrum of the rotating pressure force with the inclusion of the stochastically forced blade motion will therefore be made from the convolution of the spectrum of the deterministic portion of the rotating pressure. This process is shown schematically in Fig. 9. It can be seen that the instantaneous rotating pressure spectrum will now be made up of a series of narrowband peaks located at shaft speed, Ω, plus and minus the blade natural frequency, due to this convolution. This is a significant result as it shows the stochastic portion of the casing pressure spectrum will contain directly measureable information about blade natural frequencies.

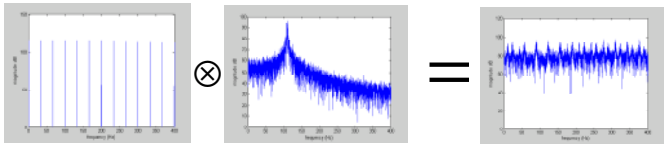

Fig. 9 Schematic of the derivation of internal pressure spectrum

Once again the casing vibration will contain the same signal properties as that of the internal pressure signal just derived, after it has passed through a LTIV filter. Results will be shown for analytically derived internal pressure and casing vibration signals along with experimental measurements taken on a simplified test rig which will now be briefly described. More information on the test rig and the data capture and post processing procedure can be found in Refs. [7, 9].

UNSW test rig

The UNSW test rig consists of a rotor arrangement with 19 flat blades, driven by an electric motor which is currently capable of running at speeds up to 2500rpm. A toroidal ring in front of the bladed arrangement, supplied with high pressure air, produces six air jets which act like trailing edge flow from upstream stator blade rows, exciting the rotor blades at multiples of shaft speed. A microphone is flush mounted in the casing in the vertical plane above the rotor blades to measure the pressure inside the casing, along with an accelerometer located at the same location to measure casing vibration, shown in Fig. 10. One blade was also instrumented with an accelerometer placed near the root of the blade, with the signal running through a set of slip rings mounted on the input shaft. The first bending, torsional and second bending mode natural frequencies were observed from the instrumented blade response spectrum and are listed in Table 3 for stationary and 1200rpm shaft speeds.

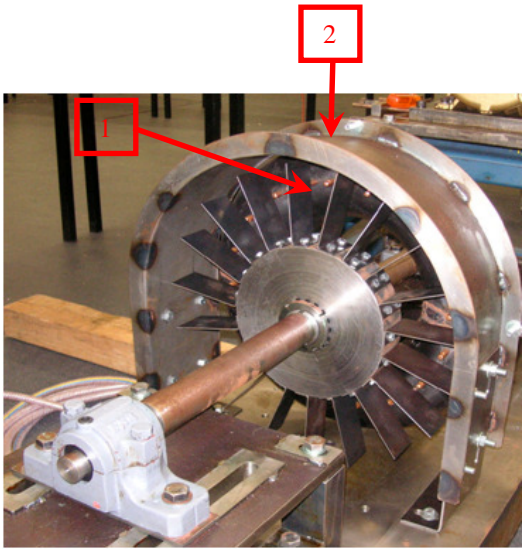

Fig. 10 Experimental test rig. (1) Air jets located on a toroidal ring which is supplied with high pressure air. (2) location of microphone and accelerometer mounting

Table 3 UNSW test rig 9th blade natural frequencies

Mode	Stationary	1200 rpm
1st bending	116.3 Hz	118.8 Hz
1st torsion	515 Hz	522.5 Hz
2nd bending	720 Hz	728.8 Hz

Direct natural frequency estimation results

The power spectrum, over a limited frequency range of the measured pressure signal, is shown in Fig. 11. The residual signal is overlaid on the synchronously averaged deterministic signal. The discrete signals can be seen to be made up of multiple discrete peaks at harmonics of shaft speed. The residual signal in Fig. 11 can be seen to be relatively flat, for the internal pressure signal, with sets of peaks spaced at multiples of shaft speed. The zoomed spectrum in Fig. 12 shows this more clearly. The casing vibration signal in Fig. 11(c) can be seen to also have other non-harmonically related peaks corresponding to the structural resonances of the casing which are excited by the internal pressure.

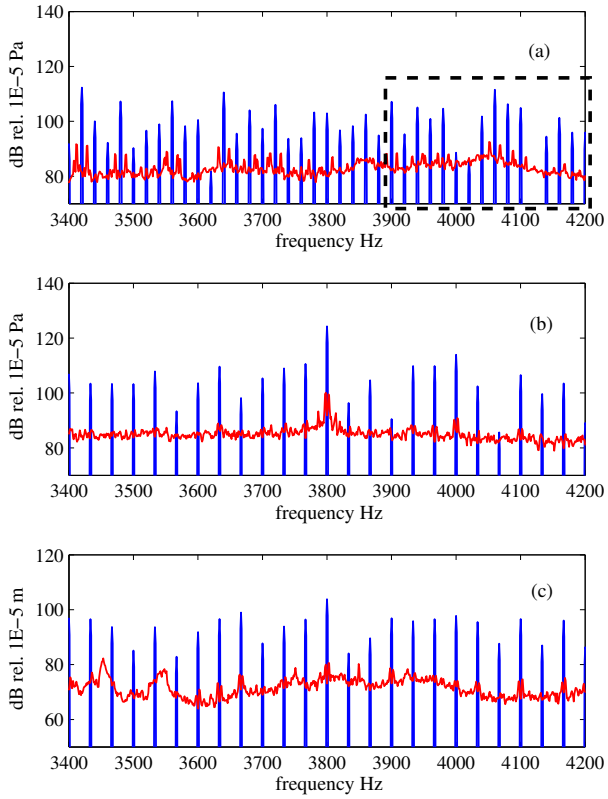

Fig. 11 Power spectrum of measured pressure and casing vibration signals, separated discrete and residual signal overlaid on each other. (a) 1200rpm pressure signal. (b) 2000rpm pressure signal. (c) 2000rpm casing vibration signal. Zoomed section indicated.

The zoomed spectrum shown in Fig. 12(a) highlights the narrow band peaks centred around multiples of shaft speed. A harmonic cursor at multiples of shaft speed is shown by the solid vertical lines; the other dashed vertical lines show the corresponding multiples of shaft speed ± the second bending mode natural frequency. Analytical results are also shown, Fig. 12(b), for the simulated pressure signal with the same operating parameters as the experimental test rig; i.e. 19 rotor blades, 6 stator blades, and 1200rpm shaft speed, and second bending mode blade natural frequency of 728.8 Hz. The same harmonic series is shown in Fig. 12(c) for the measured pressure signal and in Fig. 12(d) for the casing vibration signal with a second bending mode natural frequency estimated to be 736 Hz when the input shaft speed is running at 2000rpm. This corresponds well with the expected increase in natural frequency which would result from centrifugal stiffening, as seen in the increase in natural frequencies from stationary measurements and those at 1200rpm, cf. Table 3.

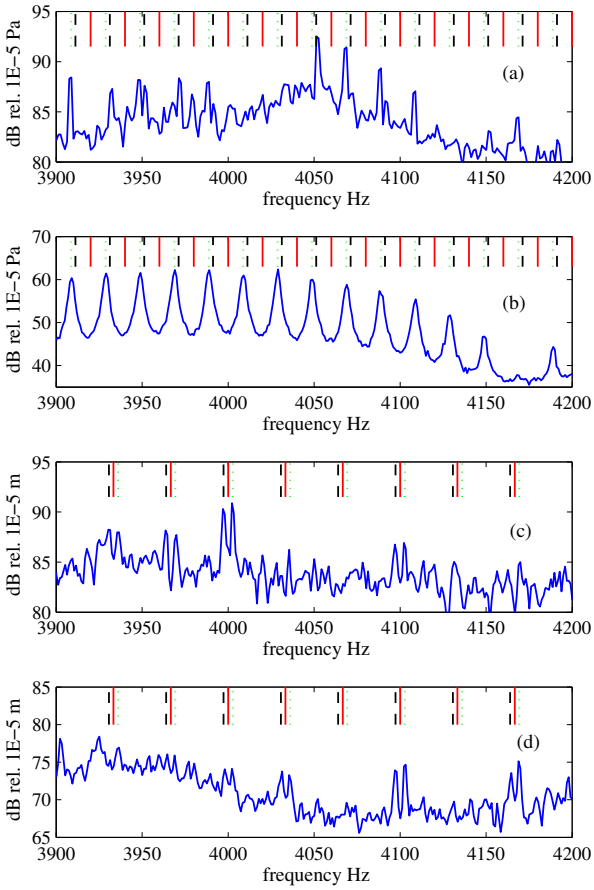

Fig. 12 Zoomed spectrum of the measured residual signals as indicated in Fig. 11 Vertical ——— line at shaft speed spacing, vertical – – – – line at shaft speed – second bending mode natural frequency, vertical ····· line at shaft speed + second bending mode natural frequency. (a) 1200rpm pressure signal. (b) 1200rpm analytical pressure signal. (c) 2000rpm pressure signal. (d) 2000rpm casing vibration signal

Within the frequency range shown for the simulated pressure signal, Fig. 12(b), only the harmonics at multiples of shaft speed minus second bending mode natural frequency are visible, which is predominantly the case also for the measured signal at 1200 rpm.

Generally it might be presumed that the first bending mode would be dominant in the response; however, as is seen, the second bending mode is the most dominantly excited blade mode visible in the measured signals, this being confirmed by measurement of the actual blade response results which can be found in Refs. [7, 9]. This is thought to be due to the fact that the pressure fluctuations are related to the acceleration of the blade rather than the displacement and as thus gives increasing weighting to higher modes and results in the second bending mode being at least as strong as the first mode.

CONCLUSIONS

The use of non-contact blade vibration measurement through the analysis of a gas turbine internal pressure and casing vibration signals was outlined in this paper.

Estimation of rotor blade vibration amplitudes from the non-conventional phase demodulation of a simulated internal pressure signal showed promise for conducting HCF estimates with a limited number of probes and providing robust amplitude estimates in the presence of measurement noise. Further research is envisaged to be undertaken with experimental verification of the effectiveness of this blade vibration measurement technique.

Measurement of rotor blade natural frequencies which could be subsequently used for the monitoring of blade health was shown to be achievable from casing vibration measurements. A significant advantage over other non-contact blade vibration measurement techniques is offered with the use of accelerometer transducers as the sensor does not need to be located within the gas flow path and are relatively easily retro mounted on existing equipment. Monitoring of the stochastic portion of the casing vibration signal also represents a noteworthy improvement over current non-contact blade vibration techniques as the analytical and experimental results showed promise in the measurement of blade natural frequencies at any engine running speed. The next step to be carried out in relation to the use of casing vibration measurements to determine rotor blade natural frequencies is an investigation into the ability of the method to isolate a single faulty blade in an experimental environment.

ACKNOWLEDGEMENTS

Grateful acknowledgment is made for the financial assistance given by the Australian Defence Science and Technology Organisation, through the Centre of Expertise in Helicopter Structures and Diagnostics at UNSW.

REFERENCES

[1] Meher-Homji, C.B. *Blading vibration and failures in gas turbines part A: blading dynamics & the operating environment*. 1995. Houston, TX, USA: ASME, New York, NY, USA.

[2] Cowles, B.A., *High cycle fatigue in aircraft gas turbines - an industry perspective.* International Journal of Fracture, 1996. **80**: p. 147-163.

[3] Lim, M.H. and M.S. Leong, *Diagnosis for loose blades in gas turbines using wavelet analysis.* Journal of Engineering for Gas Turbines and Power, 2005. **127**(2): p. 314-322.

[4] Forbes, G.L. and R.B. Randall. *Simulated Gas Turbine Casing Response to Rotor Blade Pressure Excitation*. in *5th Australasian Congress on Applied Mechanics*. 2007. Brisbane, Australia.

[5] Forbes, G.L. and R.B. Randall, *Simulation of Gas Turbine blade vibration measurement from unsteady casing wall pressure*, in *Acoustics 2009: Research to Consulting*. 2009, Australian Acoustical Society: Adelaide.

[6] Forbes, G.L. and R.B. Randall. *Detection of a Blade Fault from Simulated Gas Turbine Casing Response Measurements*. in *4th European Workshop on Structural Health Monitoring* 2008. Krakow, Poland.

[7] Forbes, G.L. and R.B. Randall. *Gas Turbine Casing Vibrations under Blade Pressure Excitation*. in *MFPT 2009*. 2009. Dayton, Ohio.

[8] Handel, P., *Properties of the IEEE-STD-1057 four-parameter sine wave fit algorithm.* IEEE Transactions on Instrumentation and Measurement, 2000. **49**(6): p. 1189-93.

[9] Forbes, G.L., *Non-contact gas turbine blade vibration monitoring using internal pressure and casing response measurements*. 2010, The University of New South Wales: PhD Dissertation. p. 211.

[10] Heath, S., *A New Technique for Identifying Synchronous Resonances Using Tip-Timing.* Journal of Engineering for Gas Turbines and Power, 2000. **122**(2): p. 219-225.

[11] Zielinski, M. and G. Ziller, *Noncontact Blade Vibration Measurement System for Aero Engine Application.* American Institute of Aeronautics and Astronautics, 2005(ISABE).

[12] Mathioudakis, K., E. Loukis, and K.D. Papailiou. *Casing vibration and gas turbine operating conditions*. 1989. Toronto, Ont, Can: Publ by American Soc of Mechanical Engineers (ASME), New York, NY, USA.